A SPECIALIZED UAV FOR SURVEILLANCE IN WINDY, TURBULENT ENVIRONMENT OF THE ANTARCTIC COAST

Zdobyslaw Goraj Warsaw University of Technology

Keywords: UAV, aircraft design, gust

Abstract

This paper presents some aspects of a project devoted to conceptual and preliminary design of a specialized UAV to be used for operation in windy, turbulent environment of the Antarctic coast for monitoring of penguins. Among important design goals were high wing loading - responsible for low sensitivity to gust and low weight-to-power ratio – important for high excess of power and quicker recovery from diving, pull-up and other manoeuvres. The design process is treated as an interdisciplinary approach, and includes a selection of thick laminar wing section, aerodynamic optimization of swept wing, stability analysis, weight balance, structural and aeroelastic analysis. many on-board redundant systems, reliability and maintainability analysis, safety improvement, performance cost and optimization. Research effort focuses mainly on platform design, selection of its external layout, control devices, structural design and on-board equipment.

1 Initial configuration – MONICA-1

A baseline configuration (swept tailless wing combined with classical fuselage developed under SAMONIT project [1,2], see Fig.1-3) will be used as a reference for more advanced **BWB** configuration, layouts, especially configuration. considered as the goal Comparisons between both configurations will be used to show the expected advantages and possible drawbacks. Assumed endurance is 5 hours, the main aircraft parts and systems weights are as follows: composite structure - 6

kg, power unit - 7 kg, communication + navigation + flight control systems - 6 kg, emergency parachute – 1 kg, payload –10 kg, fuel for 5 hours flight - 10 kg. The target airplane will have thick slotted airfoil (SA-21 type). Wing area is equal to 0.92 m², Mean Aerodynamic Chord = 0.69 m, wing span = 2 m, aerodynamic efficiency = 9.5. Stall speed at SLF is relatively high and equal to 33 m/s. Design details, technology of manufacturing processes encompassing both negative moulds and positive aircraft components, and progress in production of prototype will be shown and discussed. On-board EO/IR system is optional – either can be selected and mounted, or not, and therefore its centre of gravity (CG) is located in order not to influence the whole aircraft's CG location. Airplane will take-off from a catapult and will land in a net. Moreover, the rear part of the fuselage is used as a container for a recovery parachute. Such a recovery system offers the possibility to land in a difficult environment (where vertical falling is unavoidable), and also increases the safety factor in standard operation, an emergency. when in This two-stage parachute system consists of smaller breaking parachute (a piloting chute) and bigger recovery parachute (to be opened after a deceleration phase). Airplane is equipped with qualitative data acquisition, measurement and autopilot processing system, communication devices, as well as the ground segment consisting of data monitoring, control and navigation devices. Selected details are shown at Fig.4-10.

Aircraft is designed to be used either in closed and restricted areas or in empty, unpopulated rural areas. That decision had a big

impact on the design of the avionic system. In many countries the legal aspects of UAV operation is not yet fully solved. To get a permission to fly in restricted areas it must be shown that the vehicle will never leave the designated airspace. For this project a flight abort system was developed, which provides a guaranty that the flight can be stopped under any conditions. Therefore a parachute with a double redundant actuators, power supply and control electronic, was developed. The ejection of that system can be activated by the backup pilot, from the ground control station or automatically, if the onboard system detects a total loss of data link for a certain time. In order to also increase the reliability of the system, redundancies have also been implemented in the power supply system, wiring harness, control surface actuators, propulsion system and fuel system.

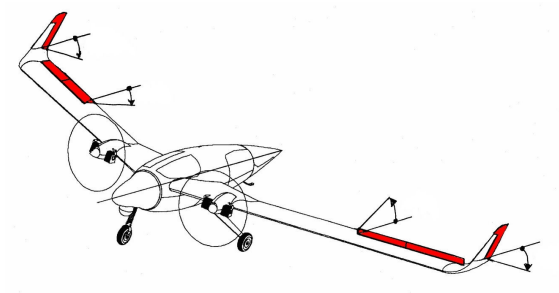


Fig.1 Baseline configuration

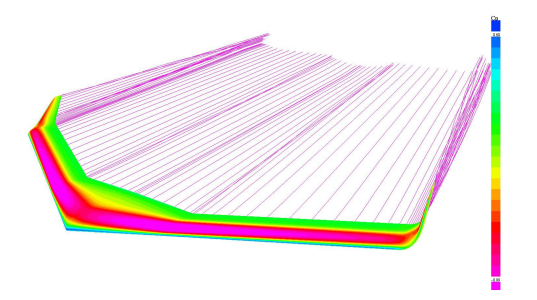


Fig.2 Pressure distribution over the wing of baseline configuration

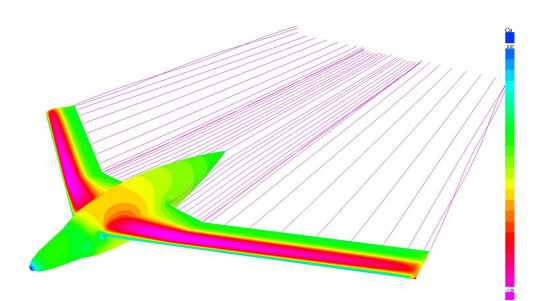


Fig.3 Pressure distribution over the wing-body



Fig.4 Slotted wing section used for BWB configuration, SA-21 type

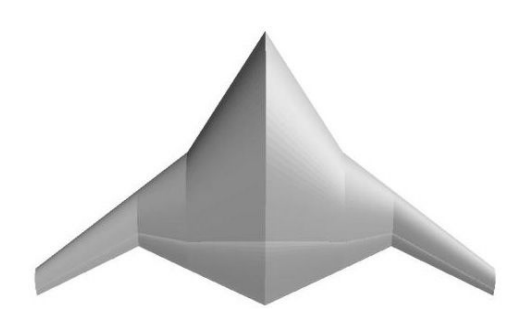


Fig.5 Initial BWB planform

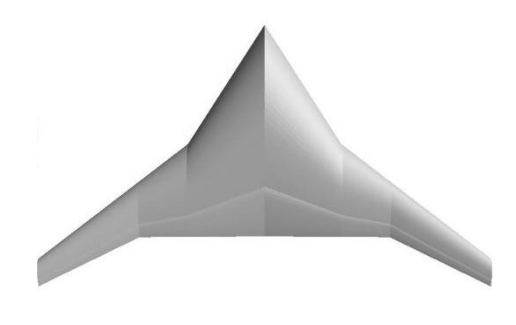


Fig.6 BWB planform after optimisation process

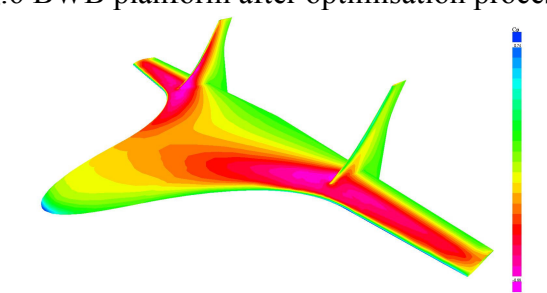


Fig.7 Initial position of vertical tailplanes

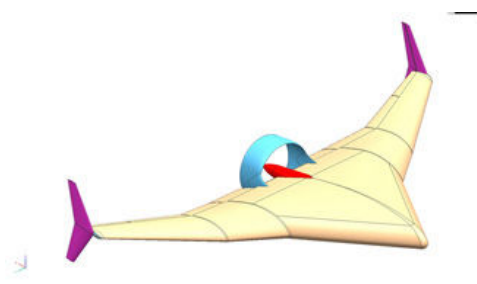


Fig.8 Aerodynamic layout – a trade-off between different aerodynamic and design requirements

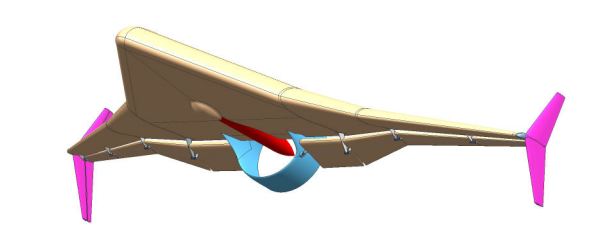


Fig.9 Side-bottom view on BWB configuration

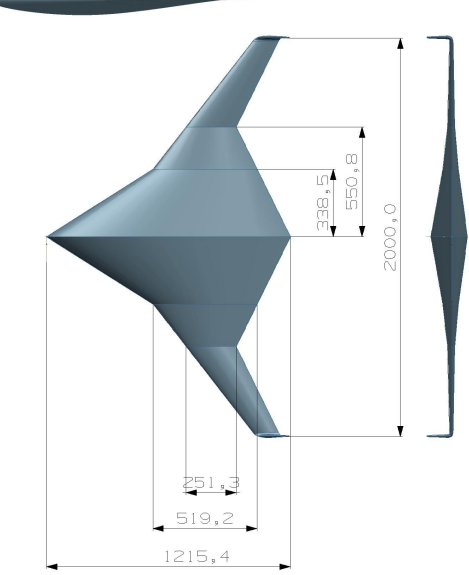


Fig.10 Initial BWB geometry assumed for aerodynamic calculation

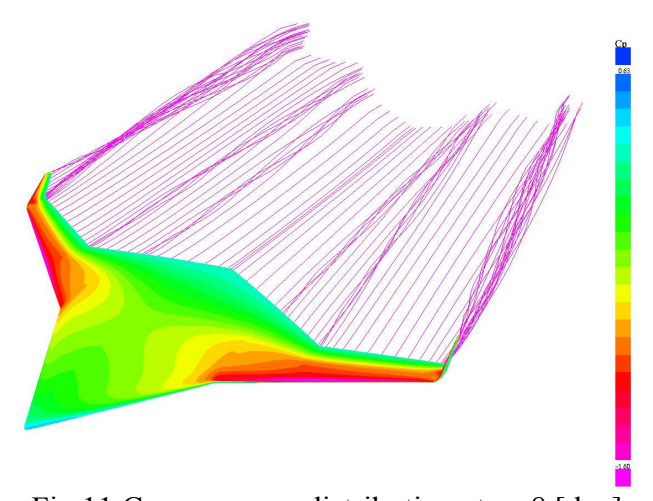


Fig.11 Cp – pressure distribution at α =8 [deg]

Basing on computed pressure distribution a number of characteristics were assessed by linear approximation

$$C_L(\alpha) = \frac{dC_L}{d\alpha} \cdot (\alpha - \alpha_0)$$

Among these characteristics there are

$$\frac{dC_L}{d\alpha}$$
 = 3,318[1/rad]=(0,0579[1/deg]);

$$\alpha_0 = -0.16^{\circ}$$
; $C_L(\alpha = 0) = 0.009$; $C_{LMAX} = 0.878$.

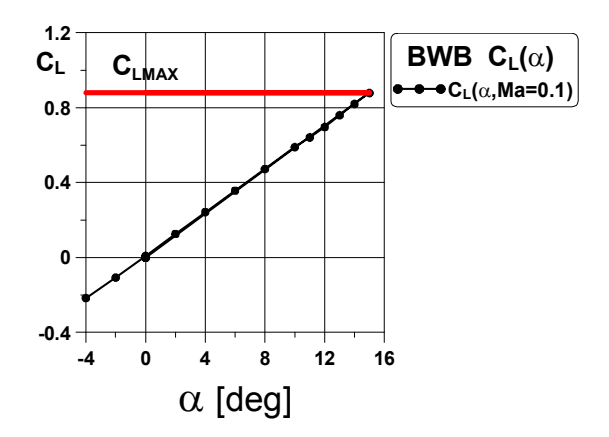


Fig. 12 Lift curve slope $C_L(\alpha)$

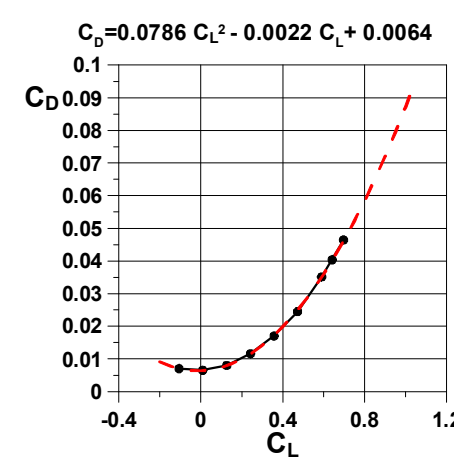


Fig. 13 Drag polar $C_L(C_D)$

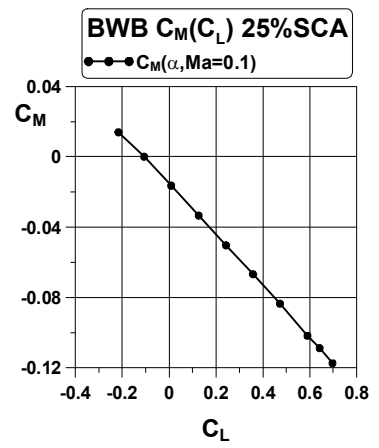


Fig.14 Pitching moment $C_M(C_L)$

Pitching moment with respect to 25% of MAC is presented at Fig.14, where

$$Cm(C_L) = \frac{dCm}{dC_L} \cdot Cz + Cm_0;$$

$$\frac{dCm}{dC_I} = -0.139$$
; $C_{m0} = -0.015$.

Lift force distribution versus wing span is presented at Fig.15. This lift distribution was analysed in order to optimise wing geometry, especially to define the wing torsion, protect ailerons against lost of control and to maximise the lift at central part of the wing.

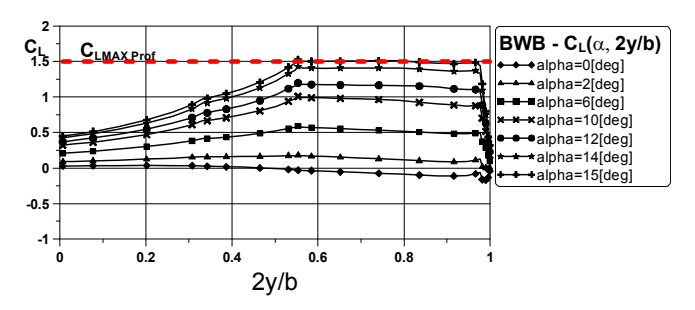


Fig. 15 Lift force distribution versus wing span

Maximum lift coefficient for wing section NACA 64₂-215 is equal to 1.5. Maximum lift coefficient computed for the whole aircraft is $C_{L,MAX}$ =0.878 and can be attained at angle of attack α =15°.

In the Tables bellow there are lift forces and pitching moments coefficients with deflected flap (F1, see Fig.16):

For δ_{F1} =-5[deg]:

α [deg]	$\mathbf{C}_{\mathbf{L}}$	C_{MY}
0	-0,00871	-0,00731
5	0,282	-0,049
10	0,557	-0,086

For δ_{F1} =-10[deg]:

α [deg]	$\mathbf{C}_{\mathbf{L}}$	C_{MY}
0	-0,023	0,000583
5	0,266	-0,040
10	0,547	-0,080

In the Tables bellow there are lift forces and pitching moments coefficients with deflected flap (F2, see Fig.16):

For δ_{F2} =-5[deg]

α [deg]	$\mathbf{C}_{\mathbf{L}}$	C_{MY}
0	-0,030	-0,000234
5	0,261	-0,042
10	0,542	-0,082

 δ_{F2} =-10[deg]

α [deg]	$\mathbf{C}_{\mathbf{L}}$	C_{MY}
0	-0.067	0.015
5	0.226	-0.027
10	0.505	-0.066

Control derivatives of lift force and pitching moments with respect to external flap (F1) deflection, computed for $\alpha=0^{\circ}$, are:

$$\frac{\partial C_L}{\partial \delta_{F1}} = 0.185 \ [1/rad](0.00323 \ [1/deg])$$

$$\frac{\partial C_{MY}}{\partial \delta_{FI}} = -0.097 \ [1/rad](-0.0017 \ [1/deg])$$

Control derivatives of lift force and pitching moments with respect to internal flap (F2) deflection, computed for $\alpha=0^{\circ}$, are:

$$\frac{\partial C_L}{\partial \delta_{F_2}} = 0.437 \ [1/rad](0.00763 \ [1/deg])$$

$$\frac{\partial C_{MY}}{\partial \delta_{F2}} = -0.180 \ [1/rad](-0.00314 \ [1/deg])$$

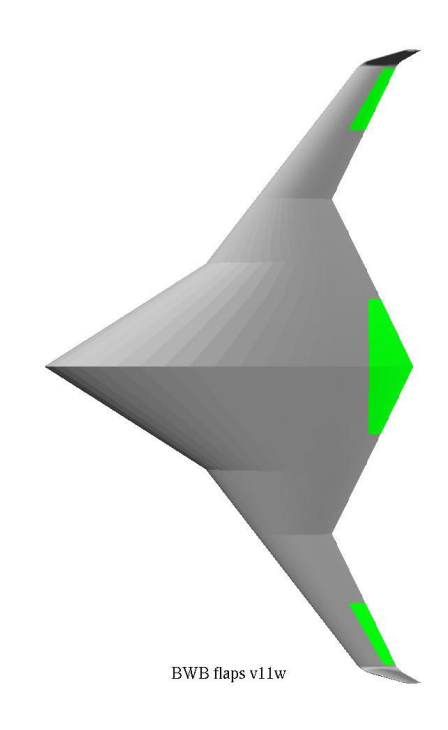


Fig.16 External (F1) and internal (F2) flaps

Lift force distribution versus wing span is presented at Fig.17. This lift distribution was analysed in order to optimise wing geometry, especially to define the wing torsion, protect ailerons against lost of control and maximise the lift at central part of the wing.

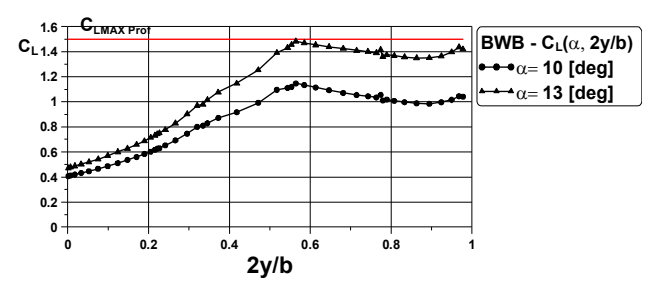


Fig.17 Lift force distribution versus wing span

Maximum lift coefficient for wing section NACA 64_2 -215 is equal to 1.5. Maximum lift coefficient computed for the whole aircraft is $C_{L,MAX}$ =0.889 and can be attained at angle of attack α =13[deg].

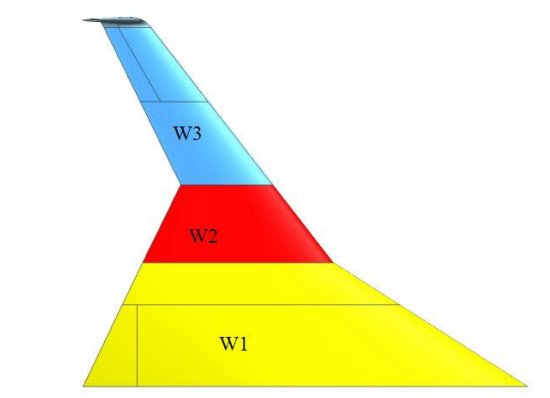


Fig. 18 Wing divided into 3 areas, W1, W2, W3

	V	V1	W	⁷ 2	V	W3
	C_{L}	C_{M}	C_{L}	C_{M}	C_{L}	C_{M}
$\alpha=10^{\circ}$	0,176	0,0118	0,084	-0,017	0,093	-0,0421
α=13°	0,208	0,0162	0,105	-0,021	0,125	-0,0559

Two different concepts of BWB (v05 and v06) were compared in order to find the one offering the highest C_L at minimum pitching moment C_M , see Fig.19.

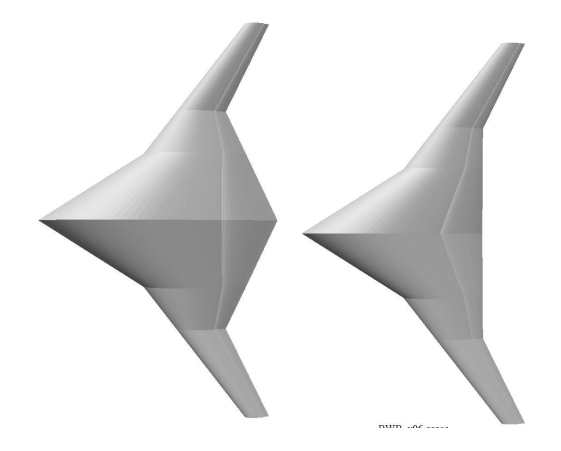


Fig.19 Two different concepts of BWB (v05 on left side and v06 on right side)

Important aerodynamic data for both configurations are shown in the table bellow:

	BWB v05	BWB v06
Wing area [m ²]	0.92	0.77
Wing span [m]	2.0	2.0
MAC [m]	0.692	0.533
X _{25%MAC}	0.582	0.567
Z _{25%MAC}	0	0
Wing section	S.A19/17	S.A19/17

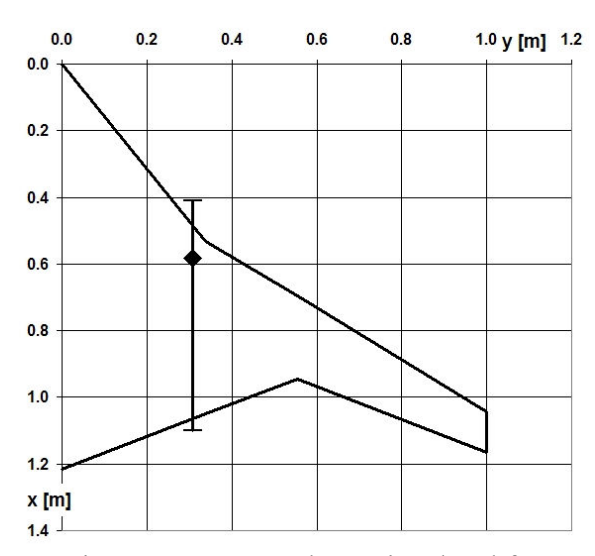


Fig.20 Mean Aerodynamic Chord for v05

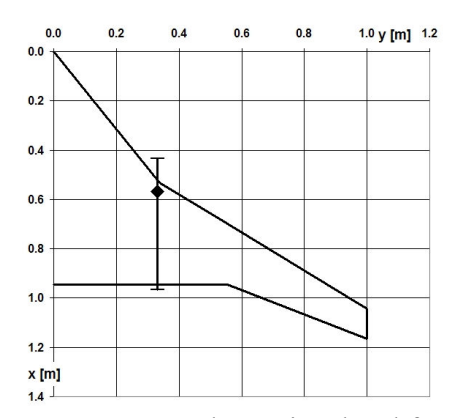


Fig.21 Mean Aerodynamic Chord for v06

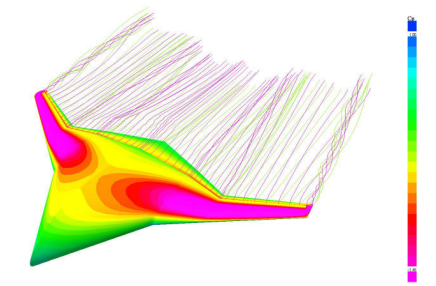


Fig.22 Pressure distribution for BWB v05 at α =4°

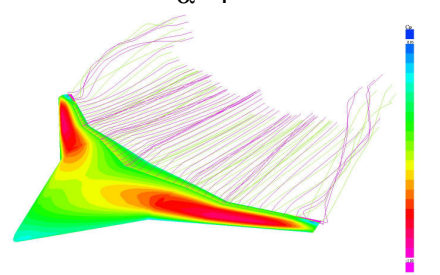


Fig.23 Pressure distribution for BWB v06 at α =4°

Aerodynamic characteristics for configurations v05 and v06 were computed by VSAERO software and are compared bellow

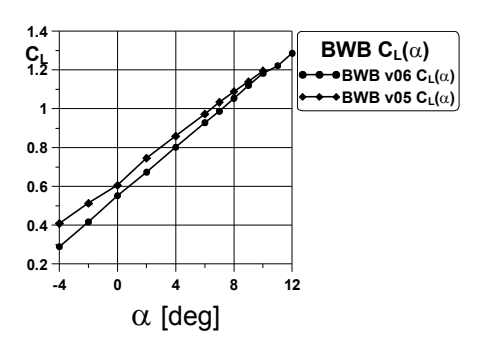


Fig.24 $C_L(\alpha)$ dla BWB v05 and v06

	v05	v06
$dC_L/d\alpha$ [1/deg]	0.0571	0.0635
$C_L(\alpha=0)$	0.628	0.547
α_0 [deg]	-10.98	-8.6

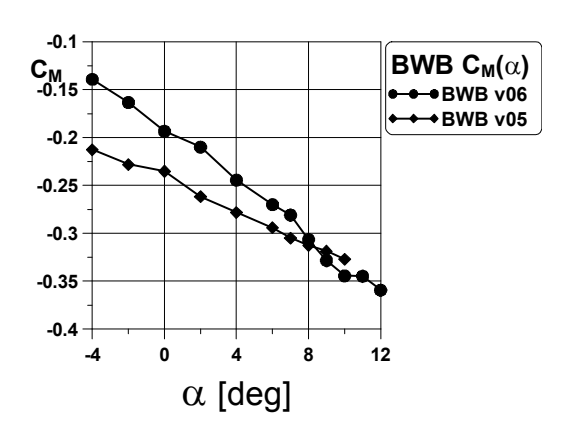


Fig.25 Pitching moment coefficients $C_M(\alpha)$ for BWB v05 and BWB v06

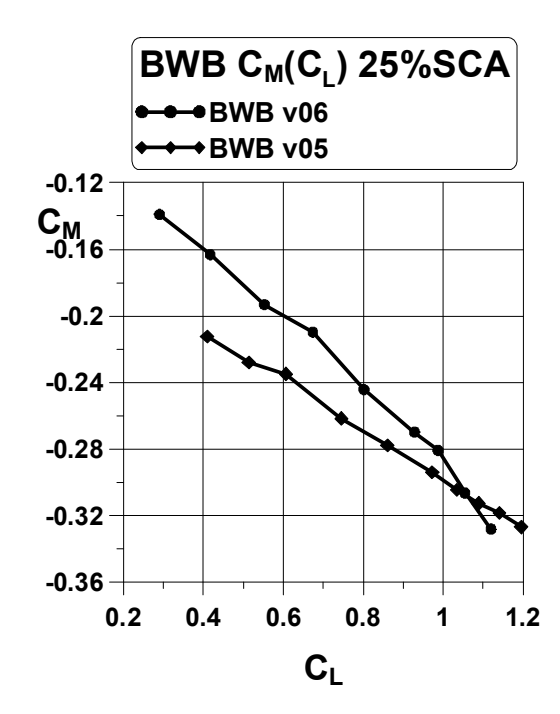


Fig.26 Pitching moment coefficients $C_M(C_L)$ for BWB v05 and BWB v06

	v05	v06
dC_{M}/dC_{L}	-0.149	-0.205
$C_{m0}(C_L=0)$	-0.15	-0.078

Aerodynamic characteristics were computed using different software packages [6], for example VSAERO (based on Panel Method), MGAERO (based on Euler code) and ANSYS (based on RANS code), see Fig.11-32. In the linear range of angles of attack (-5° < α < 10°) results of computations are fully consistent, see Fig.27-28. Some results coming from

ANSYS are presented at Fig.29-30. Internal structure and selected boundaries of design parameters, responsible for choosing the so-called design point, are shown at Fig.33-34.

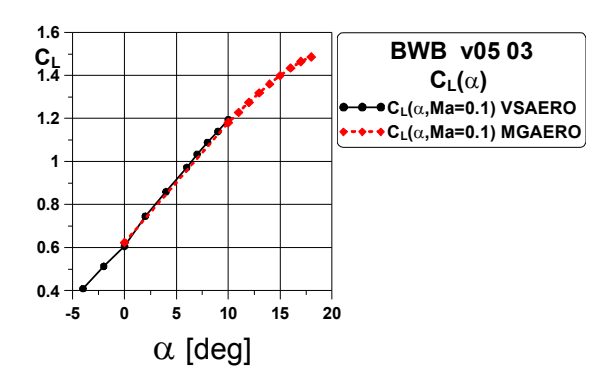


Fig.27 Lift force coefficients $C_L(\alpha)$ for BWB v05, computed by VSAERO and MGAERO

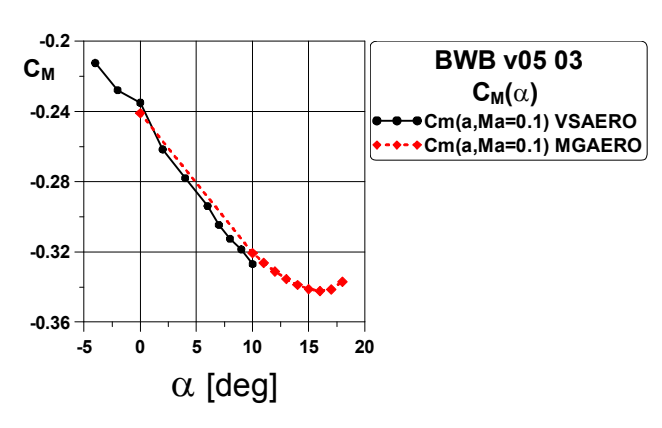


Fig.28 Pitching moment coefficients $C_M(\alpha)$ for BWB v05, computed by VSAERO and MGAERO

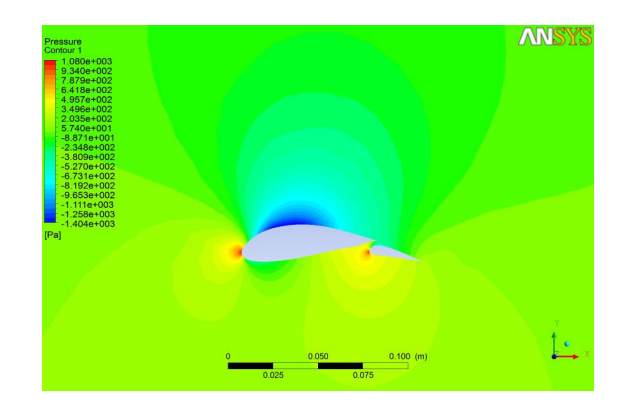


Fig.29 Pressure isolines computed within ANSYS and corresponding to flow analysis around S.A.-19 wing section proposed for v05 and v06 configurations

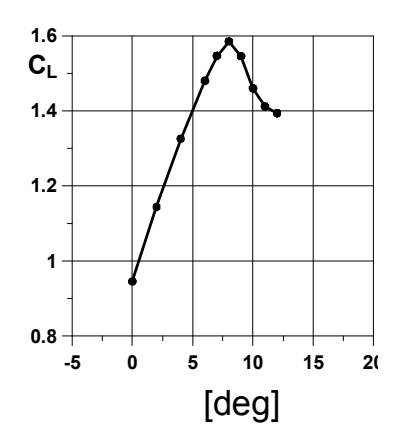


Fig.30 Lift curve slope $C_L(\alpha)$ obtained from ANSYS for wing section S.A.-19

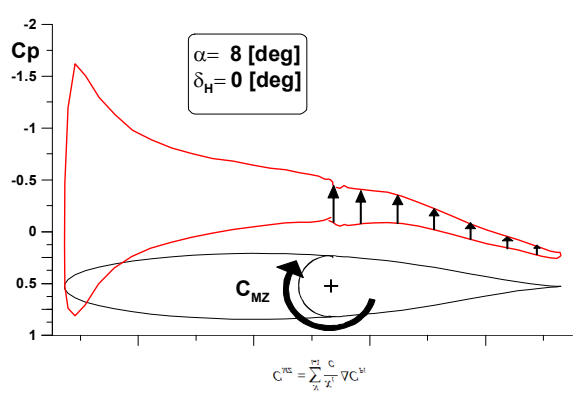


Fig.31 Pressure distribution on undeflected internal BWB flaps

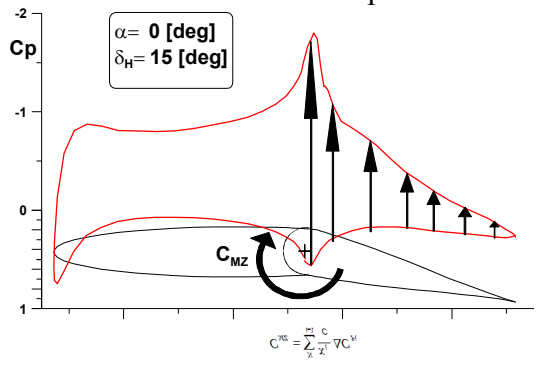


Fig.32 Pressure distribution on not deflected internal BWB flaps

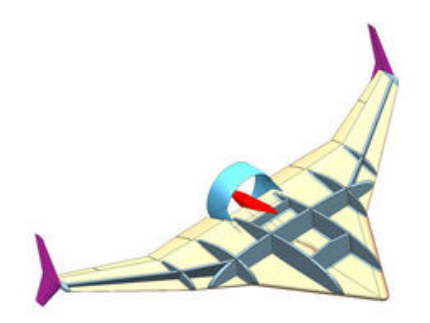


Fig.33 Internal design layout and loaded structure

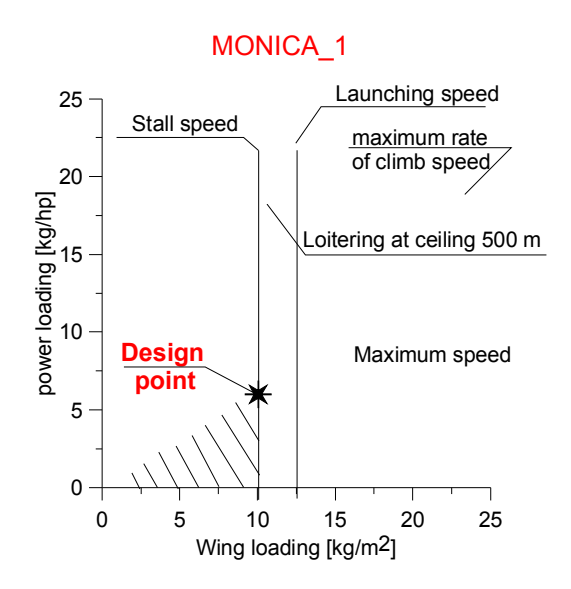


Fig.34 Selection of design parameters: wing loading and power loading

2 Traditional configuration – MONICA-2

take-off weight of **BWB** Maximum configuration is equal to 40 kg corresponding wing loading and power loading are 25 kg/m2 and 2 kg/hp, respectively. It means that relatively heavy aircraft does not offer sufficient low sensitivity to gust. Heavy aircraft means difficulties with its handling in Antarctic environment and demands a highenergy catapult. Local Reynolds number for external part of the wing for BWB configuration is relatively low (due to small local wing chord) and there is a risk that it would be of order of critical Reynolds number what can deteriorate aerodynamic efficiency of the **BWB** configuration. Moreover, after a detailed analysis of future missions we came to the conclusion that there is no need to have 5 h endurance (2 h will be sufficient) and that smaller payload will be sufficient (MONICA-1 has 10 kg payload). Taking into account all these factors we have decided to change the configuration layout from BWB into classic configuration having efficient Leading Edge Extension (LEX or strakes) to increase critical angle of attack, see Fig.35. Structure layout and location of main on-board systems are shown at Fig.36. Main aircraft parameters, three view projections and some design details are given at Fig.37-38.

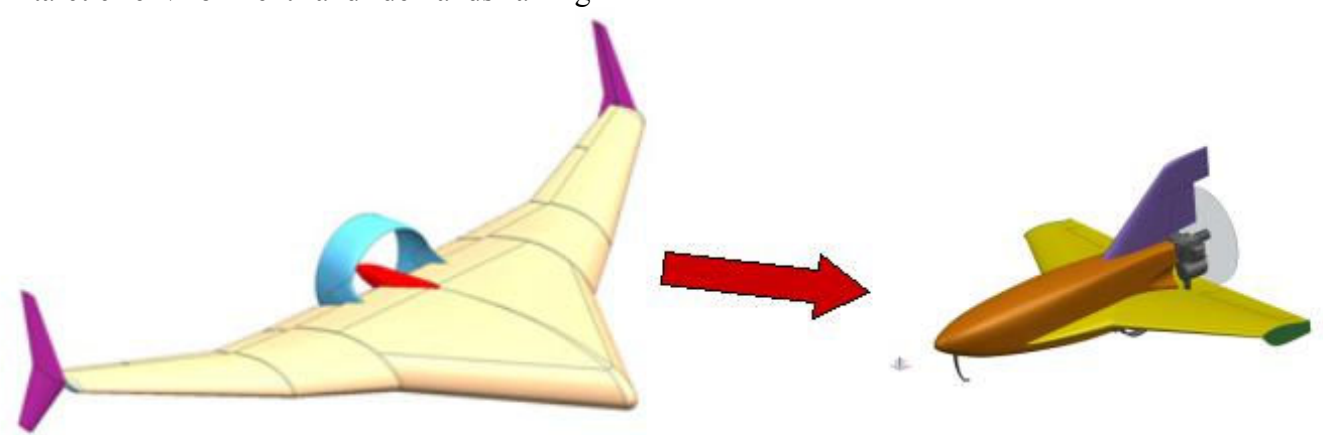


Fig.35 Change of configuration layout – from BWB to classic configuration

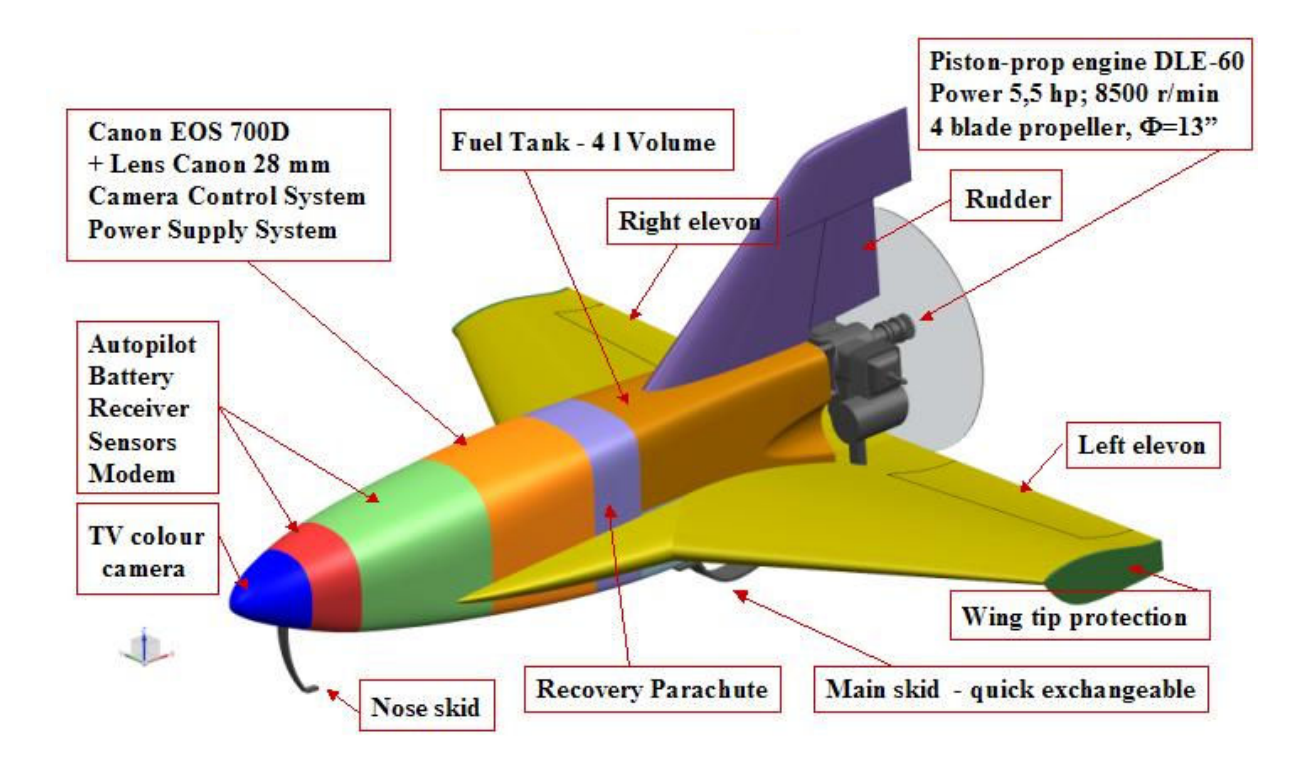


Fig.36` Structure and main on-board systems

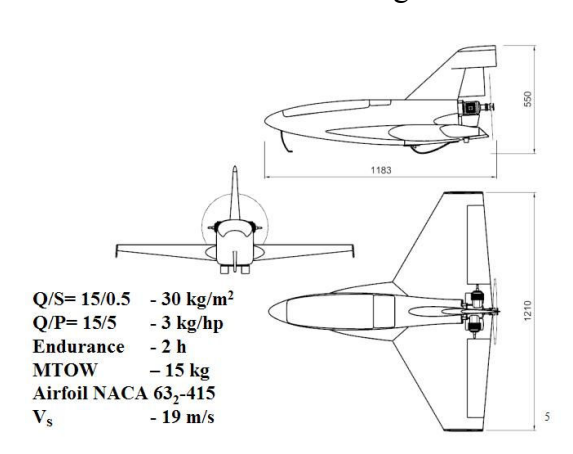


Fig.37 Main parameters and three views of the aircraft

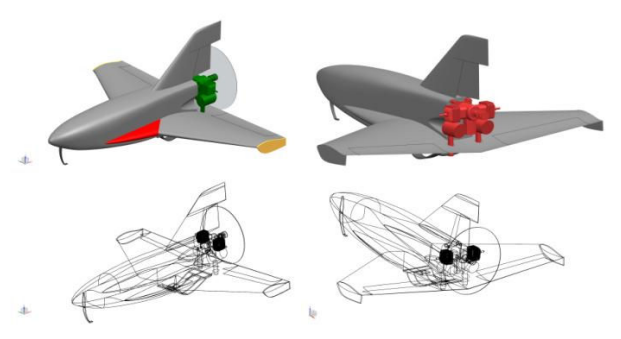


Fig.38 Wing strakes and power unit arrangement

One important feature of a UAV is its sensitivity to gust conditions. The lower the sensitivity, the better the design. Low sensitivity to gust can be achieved by high wing loading mg/S (high mg/S \rightarrow low W/W_g \rightarrow low $\Delta\alpha \rightarrow$ low n \rightarrow low sensitivity). It follows directly from the mathematical model expressed by equations (1-4).

$$\Delta \alpha = \frac{W_g - W}{V},\tag{1}$$

$$m\dot{W} = \frac{1}{2} \rho V^2 S \frac{W_g - W}{V} C_{L\alpha}$$
, (2)

$$m\dot{W} + qS\frac{C_{L\alpha}}{V}W = qS\frac{C_{L\alpha}}{V}W_g , \qquad (3)$$

$$\frac{W}{W_g} = \left(1 - e^{-\frac{q \, S \, C_{La}}{mV}t}\right), \tag{4}$$

because

$$if \ \frac{mg}{S} \ is \ high \ then \ e^{\frac{F^{\star - S}}{mg}} \ is \ low \ and \ e^{-\frac{qSC_{los}}{mV}t} = \frac{1}{e^{\frac{qSC_{los}}{mV}t}} = \frac{1}{e^{\frac{F^{\star - S}}{mg}}} \ is \ high$$

SC

$$\frac{W}{W_g} = \left(1 - e^{-\frac{qSC_{L\alpha}}{mV}t}\right) \text{ is low and } \Delta\alpha \text{ is low}$$

and load coefficient "n" is low.

Let introduce a new parameter

$$s = \frac{q \, S \, C_{L\alpha}}{m \, V} \quad , \tag{5}$$

and let request that V/V_g (see eq.4) after the time Δt get the value of ½. From the equation

$$\frac{W}{W_{o}} = (1 - e^{-st}) = \frac{1}{2}$$
, (6)

one can get the solution in the form

$$\Delta t = \frac{\ln 1/2}{-s} = \frac{\ln 2}{s} \,. \tag{7}$$

Eq. (7) was used to compute data for Fig.40.

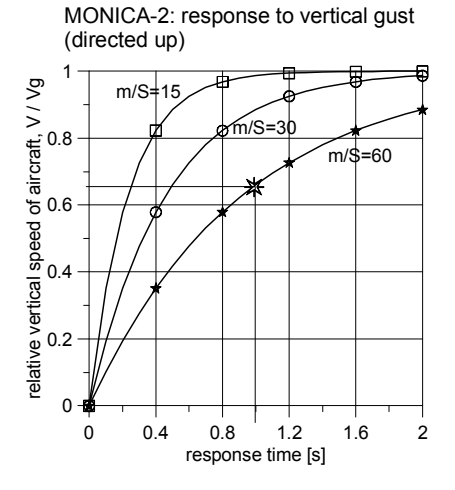


Fig.39 Aircraft response to a simple sharpedged gust, computed for MONICA-2

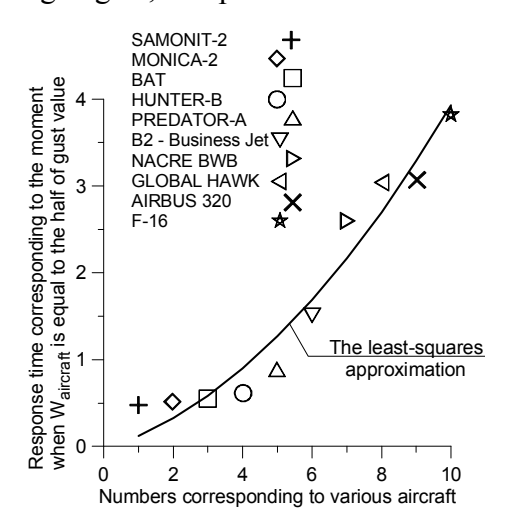


Fig.40 Aircraft response to a simple sharpedged gust, computed for different type and weight aircraft

Fig.39 presents the responses of MONICA-2 type configurations to vertical simple sharpedged gust. As it could be expected the higher

wing loading the lower relative vertical speed of the aircraft, i.e. less sensitive to gust, see also [4]. For example, after 1 s following the gust start-up the airplane vertical speed is equal to 0.6 of gust value. An essentially higher response time (i.e. lower sensitivity to gust) is possible only for much heavier aircraft, see Fig.40. An alternative approach consists in installing an Automatic Flight Control System (see for example [5]), which can reduce an impact of gust and turbulence.

3 Stability analysis

Initial configuration of MONICA-2 appeared to be dynamically unstable. Stability analysis was performed basing on a linearised mathematical model [1,3] and considering small disturbances around steady state solution (trim conditions, Fig.41). Centre of gravity of the aircraft in its configuration (Fig.42) is relatively high ($z_C=14\%$) with respect to Mean Aerodynamic Chord (MAC). This results in unstable Dutch Roll mode, see Fig.42. In order to stabilise the Dutch Roll mode the wing dihedral angle was increased from 1° to 6° and the engine was shifted down. Fig. 42-46 present a sequence of results (configurations from no 1 to no 5) which show how stable Dutch Roll mode was achieved. There were used the following symbols: l_v - horizontal arm of vertical tail; z_v – vertical arm of vertical tail; S_{vu} - reference area of vertical tail.

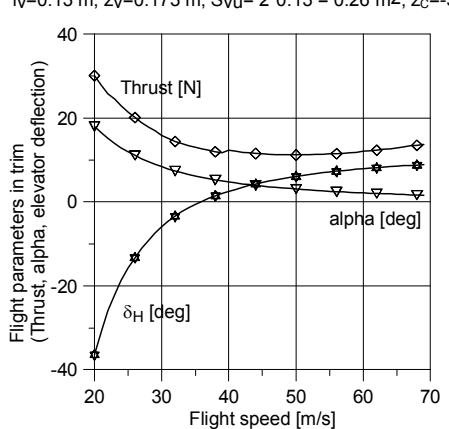


Fig.41 Flight parameters in trim – starting point for stability analysis

MONICA-2 Unstable Dutch Roll, initial configuration - no 1 l_V =0.123 m; z_V =0.272 m; S_V u= 1*0.13 = 0.13 m²; z_C =+14%

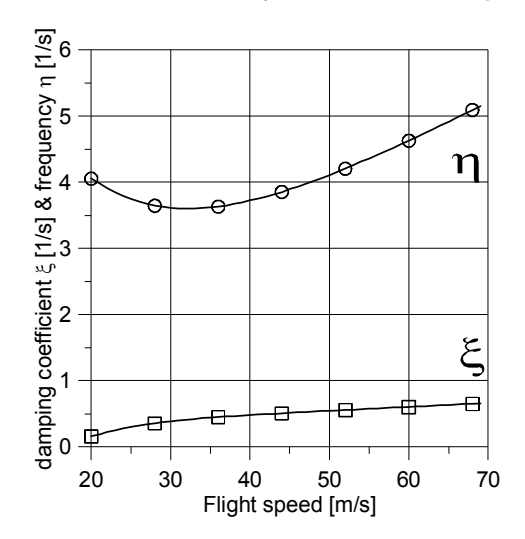


Fig.42 Initial dynamically unstable configuration (no 1) with high location of CG – Z_C =+14% of MAC

MONICA-2 Unstable Dutch Roll, configuration - no 2 I_V =0.123 m; Z_V =0.272 m; S_V =1*0.13 = 0.13 m²; Z_C =+7%

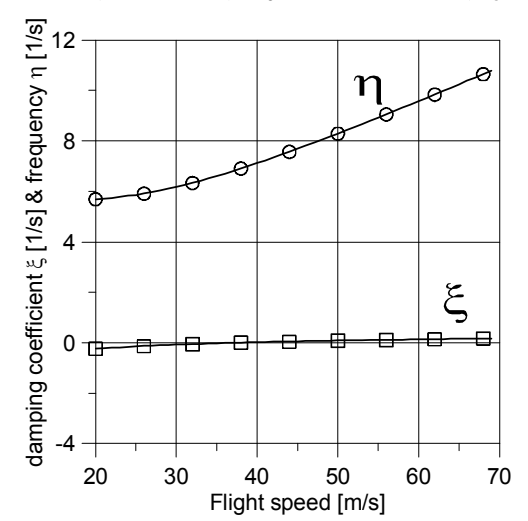


Fig.43 Dynamically unstable configuration (no 2) with high location of $CG - Z_C = +7\%$ of MAC

MONICA-2 Dutch Roll, configuration - no 3 $l_y=0.123$ m; $z_y=0.272$ m; $S_{yu}=1*0.13=0.13$ m²; $z_c=+4\%$

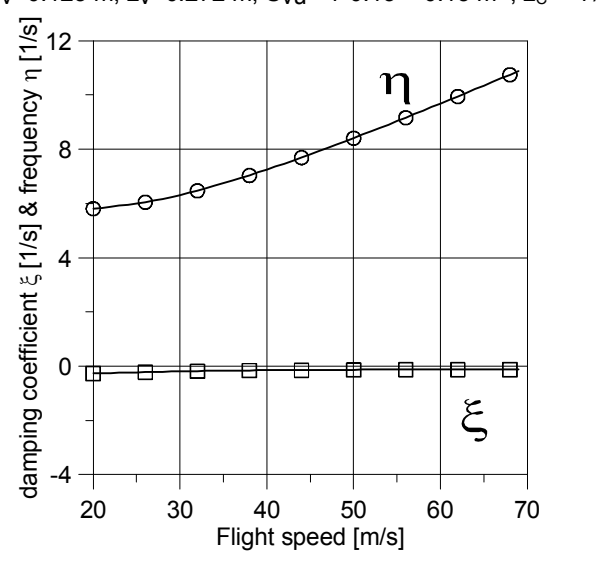


Fig.44 Stable configuration (no 3) with high location of $CG - Z_C = +4\%$ of MAC. Stability margin is very low

MONICA-2 stable Dutch Roll, configuration - no 4 I_V =0.123 m; z_V =0.272 m; S_{VU} = 2*0.13 = 0.26 m²; z_C =+2% average wing dihedral = +5°

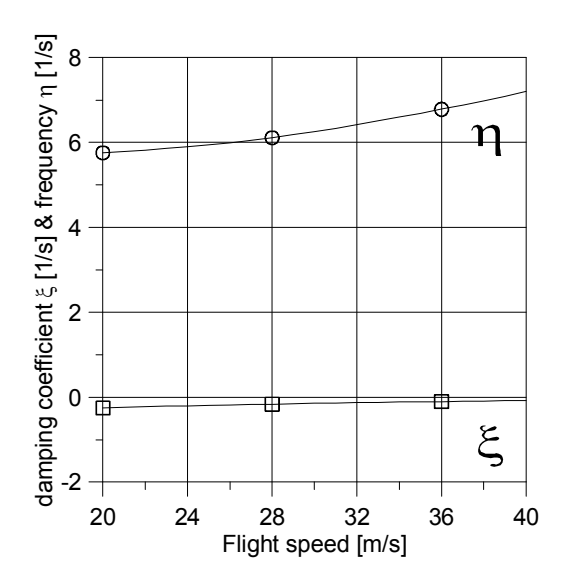


Fig.45 Stable configuration (no 4) with high location of $CG - Z_C = +4\%$ of MAC. Stability margin is higher but still too low

MONICA-2 Stable Dutch Roll, final configuration - no 5 $I_V=0.13$ m; $z_V=0.173$ m; $S_{VU}=2*0.13=0.26$ m²; $z_C=-5\%$

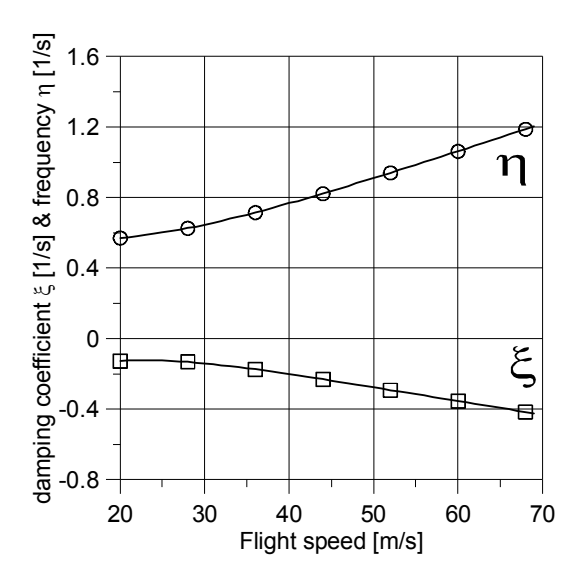


Fig.46 Stable configuration (no 3) with high location of CG – Z_C = -5% of MAC. Stability margin sufficient to fly safely

Conclusion

Light UAV are very sensitive to gust and designers have a limited spectrum of possible choices to make these airplanes more resistant against gust disturbances. It is much easier to increase power-to-weight ratio (to speed-up recovery from gust-following manoeuvres) and to increase the critical angle of attack (to protect the aircraft against the stall). Due to small local chord of the BWB configuration and high risk of decreasing of aerodynamic efficiency it was decided that classic streaked Delta wing with tailplane will offer better aerodynamic and dynamic properties for the mission in windy, turbulent environment. Flight tests are planned to be performed both in Europe and in Antarctic cost and they will finally confirm all these theoretical considerations.

References

[1] Goraj Z., Rodzewicz M., Grendysa W., Jonas M., Design and configuration layouts of an advanced long endurance UAV- lessons learnt after flight testing. 28th International Congress of the Aeronautical Sciences, Brisbane, Sept. 2012, paper.763.

- [2] Goraj Z., Lessons learnt from SAMONIT program a long endurance, surveillance, light UAV. Proceedings of READ Conference, Brno, Oct.2012, paper no 8.
- [3] Goraj Z., Flight Dynamics models used in different national and international projects. *Aircraft Engineering and Aerospace Technology*, Vol. 86, Iss: 3, pp.166-178, 2014.
- [4] ESDU, An introduction to rigid aeroplane response to gusts and atmospheric turbulence. *ESDU 04024*, London Nov. 2004 with Amendments A and B, June 2010.
- [5] Mohamed A, et al., The attitude control of fixed-wing MAVS in turbulent environments. *Progress in Aerospace Sciences*.Vol.66, No. 2, pp. 37–48, 2014.
- [6] Figat M., Aerodynamic characteristics of Penguin configuration. *Internal, unpublished report on BWB configurations, Warsaw University of Technology, Dec-April* 2013.

Contact Author Email Address: Zdobyslaw Goraj, goraj@meil.pw.edu.pl

Copyright Statement

The authors confirm that they, and/or their company or organization, hold copyright on all of the original material included in this paper. The authors also confirm that they have obtained permission, from the copyright holder of any third party material included in this paper, to publish it as part of their paper. The authors confirm that they give permission, or have obtained permission from the copyright holder of this paper, for the publication and distribution of this paper as part of the ICAS 2014 proceedings or as individual off-prints from the proceedings.

Acknowledgement

Thanks to the project No 197810 (grant agreement POL-NOR/197810/84/2013) entitled "A novel approach to monitoring the impact of climate change on Antarctic ecosystems" in the Research Programme of the EEA/Norway Grants Framework.